Zinc Finger Protein, *Hzf*, Is Required for Megakaryocyte Development and Hemostasis

Yuki Kimura,[1] Adam Hart,[1] Masanori Hirashima,[1] Chen Wang,[2] Doug Holmyard,[2] Jackie Pittman,[2] Xin-Li Pang,[1] Carl W. Jackson,[3] and Alan Bernstein[1, 4, 5]

[1]*Samuel Lunenfeld Research Institute, and the* [2]*Department of Pathology, Mount Sinai Hospital, Toronto, Ontario, M5G 1X5, Canada*

[3]*The Division of Experimental Hematology, St. Jude Children's Research Hospital, Memphis, TN 38105*

[4]*Department of Medical Genetics and Biophysics, University of Toronto, Toronto, Ontario, M5S 1A8, Canada*

[5]*Canadian Institutes of Health Research, Ottawa, Ontario, K1A 0W9, Canada*

Abstract

Using an expression gene trapping strategy, we recently identified a novel gene, hematopoietic zinc finger (*Hzf*), which encodes a protein containing three C_2H_2-type zinc fingers that is predominantly expressed in megakaryocytes. Here, we have examined the in vivo function of *Hzf* by gene targeting and demonstrated that *Hzf* is essential for megakaryopoiesis and hemostasis in vivo. *Hzf*-deficient mice exhibited a pronounced tendency to rebleed and had reduced α-granule substances in both megakaryocytes and platelets. These mice also had large, faintly stained platelets, whereas the numbers of both megakaryocytes and platelets were normal. These results indicate that *Hzf* plays important roles in regulating the synthesis of α-granule substances and/or their packing into α-granules during the process of megakaryopoiesis.

Key words: α-granules • hemorrhage • hemostasis • megakaryopoiesis • thrombopoiesis

Introduction

During hematopoiesis, anucleate platelets are generated from megakaryocytes and have an essential role in maintaining hemostasis in vivo. During megakaryocyte differentiation, megakaryocyte-restricted progenitor cells commence an unusual process, terminal endomitosis, in which DNA replication occurs but neither the nucleus nor the cell undergoes division (1). Hence, mature megakaryocytes are invariably polyploid, containing 4N to 64N of the normal diploid amount of DNA (2). Because platelets can produce only limited amounts of proteins, their cytoplasmic structures, including characteristic granules, are mostly derived from megakaryocytes (3). Morphologically, four distinct categories of granules differing in their internal constituents are produced by maturing megakaryocytes: α-granules, dense granules, lysosomal granules, and microperoxisomal granules (3). The α-granules, which are the most numerous, contain various proteins, including platelet-derived growth factor (PDGF)*, platelet factor 4, and von Willebrand factor (vWF). These proteins are synthesized in megakaryocytes and then transported to α-granules. These packed α-granules are subsequently shed from megakaryocytes (4). Thus, the process of megakaryocyte differentiation involves a complex series of cellular processes that culminate in the generation of functionally mature platelets.

Genetic approaches involving gene targeting in mice have revealed several genes and their protein products that are essential for megakaryopoiesis. These include various transcription factors, such as p45 NF-E2 (5), *maf*G (6), GATA-1 (7), and *Fli*-1 (8). The transcription factor NF-E2 is a heterodimer of two proteins, p45 and p18, that are members of the Cap'n'Collar protein and Maf subfamilies, respectively (9, 10). Deficiency of the p45 NF-E2 gene blocks completion of megakaryopoiesis and results in the

A. Hart's present address is The Walter and Eliza Hall Institute, PO Royal Melbourne Hospital, VIC 3050, Australia.

X.-L. Pang's present address is Arius Research, Inc., Mississauga, Ontario, L4V 1N3, Canada.

Address correspondence to Alan Bernstein, Samuel Lunenfeld Research Institute of Mount Sinai Hospital, 600 University Ave., Rm. 982, Toronto, Ontario, Canada, M5G 1X5. Phone: 416-586-8273; Fax: 416-586-8857; E-mail: bernstein@mshri.on.ca

**Abbreviations used in this paper:* AChE, acetylcholinesterase; ES, embryonic stem; GP, glycoprotein; GPS, gray platelet syndrome; *Hzf*, hematopoietic zinc finger; IRES, internal ribosome-entry site; MGDF, megakaryocyte growth and development factor; *neo*, neomycin resistant gene; PDGF, platelet-derived growth factor; TPO, thrombopoietin; vWF, von Willebrand factor.

complete absence of platelets (5), whereas the absence of MafG leads to hyperproliferation of megakaryocytes and mild thrombocytopenia (6). Mice carrying megakaryocyte-specific deletion of the GATA-1 zinc finger protein exhibit severely impaired cytoplasmic maturation of megakaryocytes and reduced platelet numbers (7). Mice carrying a null mutation in *Fli*-1, a member of the *ETS* family of winged helix-turn-helix transcription factors, exhibit a block in megakaryocyte differentiation (8).

The process of megakaryocyte differentiation also requires the interaction between thrombopoietin (TPO), also known as megakaryocyte growth and development factor (MGDF), and its cognate receptor c-Mpl (11–18). The ligand TPO/MGDF increases megakaryocyte ploidy at low concentrations while the final stage of platelet release is not dependent on TPO/MGDF (19). c-*mpl*–deficient mice exhibit thrombocytopenia and impaired megakaryopoiesis (20, 21). In addition, TPO/MGDF null mutant mice have decreased number of both platelets and megakaryocyte progenitors, and lower ploidy levels of megakaryocytes (22). Interestingly, both c-Mpl and TPO/MGDF null mice do not exhibit a bleeding disorder, suggesting that platelets produced from the abnormal megakaryocytes in these mice can function normally.

Using an approach that we have termed 'expression gene trapping,' we have previously identified and mutated in embryonic stem (ES) cells a number of genes that are expressed in hematopoietic and/or endothelial cells in vitro and in vivo (23, 24). One of these genes, hematopoietic zinc finger (*Hzf*), encodes a novel zinc finger protein which is predominantly expressed in megakaryocytes (24). Mice homozygous for the gene trapped allele of *Hzf* ($Hzf^{gt/gt}$) exhibit no obvious phenotype (24). Transcripts corresponding to the *Hzf* gene were detected in $Hzf^{gt/gt}$ mice, consistent with the possibility that the trapped *Hzf* allele generated in our previous study was not a null allele. Therefore, to investigate the in vivo role of *Hzf*, we generated mice with a null *Hzf* mutation by gene targeting. Here we describe the essential function of *Hzf* in α-granule formation and megakaryopoiesis.

Materials and Methods

Generation of $Hzf^{-/-}$ Mutant Mice. DNA fragments corresponding to the murine *Hzf* gene fragments were cloned from a 129/Sv genomic DNA library using a mouse *Hzf* cDNA probe (24). 17 overlapping phage genomic clones containing exons encoding three zinc finger domains were isolated. A targeting vector was designed to replace a 5.5-kb genomic fragment including the exons encoding three zinc finger domains with an internal ribosome-entry site (IRES) *Lac*Z and a neomycin resistant gene (*neo*). IRES *Lac*Z and *neo* were inserted in the pPNT targeting vector in the sense orientation to *Hzf* transcription, such that IRES *Lac*Z was flanked on the 3′ side by 1.6 kb of genomic DNA and that *neo* was flanked on the 5′ side by 4.5 kb of genomic DNA. The targeting vector was linearized with *Not*I and electroporated into R1 ES cells. After positive-negative selection with gancyclovir and G418, 800 surviving clones were picked and screened by Southern blot analysis. Three out of six homologous recombinant ES clones were aggregated into CD1 blastomeres and transferred to foster mothers to generate chimeras. Chimeric mice were mated with CD1 females, and germline transmission of the mutant allele was verified by PCR and Southern blot analysis of ear punched tissues and tail DNA from F1 offspring. A primer "a" and "b" specific for the *Hzf* gene (5′-GGACCCTGTACAGAAAGCTGT-3′ and 5′-GCTTGGTC-TACAGAGTGATT-3′, respectively) and a primer "c" specific for the IRES gene (5′-GGAGGGAGAGGGGCGGAATT-3′) were used in PCR analysis. Germline transmission of the targeted *Hzf* allele was achieved for three independent ES clones. F2 offspring from heterozygous intercrosses were genotyped by Southern blotting. Mutant mice derived from three targeted ES cells showed the identical phenotype.

Histological Analysis. Organs were isolated in ice-cold PBS 3 wk after birth, fixed overnight in 4% paraformaldehyde at 4°C (for brains, fixed at least 1 wk in 4% paraformaldehyde at 4°C), dehydrated, and embedded in paraffin. Sections 5-μm thick were cut and stained with hematoxylin and eosin.

Hematological Analysis. 4-wk-old mice were anesthetized with methoxyflurane. Peripheral blood was collected by heparinized capillary puncture of the retroorbital venous plexus into a tube containing 5 μl of 0.5 M EDTA, pH 8.0 (Becton Dickinson). Peripheral blood cell counts were determined with MASCOT automated hematology system (CDC Technologies). Blood smears and bone marrow smears were stained with Wright-Giemsa stain.

The preparation of platelets was performed essentially as described previously (25). Peripheral blood, which was prepared as described above, was centrifuged at 300× *g* for 10 min at room temperature to obtain platelet-rich plasma. The platelets were washed three times with PBS by centrifugation at 1,300× *g* for 10 min and were used immediately for Western immunoblot analysis.

Bleeding Time Assays. Bleeding times were measured as described previously (26, 27) using 4-wk-old mice. 2 mm of the tip at the tail was cut with a sharp scalpel blade, the tail was placed in a solution of saline at 37°C, and the time for the flow of blood to cease was recorded. Genotyping of the animals took place after this procedure so that tails were intact for bleeding-time measurements. If bleeding restarted within 1 min, this result was recorded as a rebleed and taken to indicate an unstable hemostatic event.

Measurements of Megakaryocyte Frequency and DNA Content. DNA distribution of megakaryocytes in unfractionated bone marrow cells was determined as described previously (2, 28). Bone marrow cells were harvested from *Hzf* mutant and control mice.

CFU-Mk Assay. Megakaryocyte progenitor cells, in the bone marrow from *Hzf* mutant and control mice, were assayed in collagen-based media (StemCell Technologies) supplemented with recombinant human TPO (50 ng/ml), IL-6 (20 ng/ml), IL-11 (50 ng/ml), and recombinant mouse IL-3 (10 ng/ml). Colonies were stained for acetylcholinesterase (AChE) activity counted after 6 d incubation.

Ultrastructural Studies. Freshly excised spleens obtained from 3–5-wk-old $Hzf^{-/-}$ and control mice were fixed in 2% glutaraldehyde (Canemco, Inc.) in 0.1 M sodium cacodylate buffer, pH 7.3, (Canemco, Inc.). Samples were washed with 0.1 M sodium cacodylate buffer, pH 7.3, postfixed with 1% osmium tetroxide in 0.1 M sodium cacodylate buffer, pH 7.3, dehydrated in graded ethanols, and embedded in spurr epoxy resin (Canemco, Inc.). Embedded tissues were sectioned with an RMC 6000 ultramicrotome, (RMC-EM), stained with uranyl acetate, lead citrate,

and examined in a Philips CM 100 electron microscope (Philips Electron Optics).

For platelet analysis, blood was collected into a syringe with prewarmed 2% glutaraldehyde (Canemco, Inc.) in 0.1 M sodium cacodylate buffer, pH 7.3 (Canemco, Inc.), from the inferior vena cava of anesthetized mice. Immediately, the syringe was inverted several times and was set at room temperature for 2 h. Platelet-rich plasma was prepared as described above and then analyzed, as described previously (29).

For quantitative estimation of vacant α-granules in platelets, dense and vacant α-granules were counted in platelets from $Hzf^{+/+}$ and $^{-/-}$ mice by observers blinded to the experiment. The frequency of vacant α-granules was calculated from the number of detected vacant α-granules divided by that of dense α-granules.

To estimate the levels of PDGF-A in megakaryocytes, freshly excised spleens obtained from 3–5-wk-old $Hzf^{-/-}$ and control mice were fixed in 0.1 M sodium cacodylate buffer, pH 7.3 containing a combination of 0.1% glutaraldehyde (Canemco, Inc.) and 4% paraformaldehyde (Canemco, Inc.). The samples were washed with the same buffer, dehydrated with graded ethanol, infiltrated in lowicryl (Canemco, Inc.), and polymerized under UV at –20°C overnight. The sections were rinsed with PBS containing 0.15% glycine and 0.5% BSA, washed with 0.5% BSA in PBS, and then reacted with anti–PDGF-A antibody (Santa Cruz Biotechnology, Inc.) for 1 h at 22°C. After washing with 0.5% BSA in PBS, the sections were treated with anti–rabbit IgG conjugated with 10-nm gold (Amersham Pharmacia Biotech). After washing with 0.5% BSA in PBS, PBS, and H_2O, the sections were stained with uranyl acetate, lead citrate, and examined in the Philips CM 100 electron microscope. Then, PDGF-A labeling by counting the gold particles was determined as described previously (30). Briefly, the field ($3.35 \times 2.7\ \mu m^2$) from the immunogold stained sections were determined with a minimum of 10 high power field counted per mouse. The frequency of PDGF-A gold particles in α-granules was calculated from the number of detected gold particles in α-granules divided by that in the whole field.

Western Blot Analysis. Bone marrow cells were isolated from 4-wk-old $Hzf^{+/+}$ and $Hzf^{-/-}$ mice, after washed with PBS, and subsequently suspended in lysis buffer (25). Soluble fractions from each sample were boiled with sample buffer for SDS-PAGE. Eluted proteins were separated by electrophoresis and transferred to nitrocellulose membranes (Schleicher & Schuell). Immunoblotting was performed as described previously (25). We evaluated AChE expression to ensure equivalent sample loading. Commercially available Abs to vWF (Dako), fibrinogen (ICN Biochemicals), PDGF-A (Santa Cruz Biotechnology, Inc.), PDGF-B (Santa Cruz Biotechnology, Inc.), and AChE (Santa Cruz Biotechnology, Inc.) were used at the concentrations of 57 μg/ml, 160 μg/ml, 5 μg/ml, 5 μg/ml, and 5 μg/ml, respectively. Goat anti–rabbit IgG Ab-conjugated with HRP and donkey anti–goat IgG Ab conjugated with HRP were purchased from Bio-Rad Laboratories and Santa Cruz Biotechnology, Inc., respectively. The signals were visualized with an enhanced chemiluminescence detection system (Amersham Pharmacia Biotech) as directed by the manufacturer.

The detection of platelet proteins was performed basically as described previously (25). Briefly, washed platelets were lysed with the same lysis buffer, as described above. Whole platelets were treated with standard sample buffer and loaded onto 10% SDS-PAGE following the same protocol as described above. We evaluated glycoprotein (GP)IIb to ensure equivalent platelet protein loading. The anti–mouse GPIIb mAb and anti–rat IgG Ab conjugated with HRP were purchased from BD PharMingen and Santa Cruz Biotechnology, Inc., respectively. The anti-GPIIb mAb and the anti–rat IgG Ab conjugated with HRP were used at the concentrations of 0.25 μg/ml and 0.8 μg/ml, respectively. The signal-enhancement was performed as described above.

RT-PCR Analysis. Bone marrow cells, from male $Hzf^{+/+}$ and $Hzf^{-/-}$ mice, were used for RNA extraction and cDNA synthesis, as described previously (31). The detailed method for RT-PCR and the primer sequences were described elsewhere (5, 32). We equalized cDNAs from male $Hzf^{+/+}$ and $Hzf^{-/-}$ bone marrow cells by RT-PCR of hypoxanthine phosphoribosyl transferase. The RT-PCR products were analyzed by PAGE.

Statistical Analysis. Data were analyzed by using Student's *t* test. Values of $P < 0.05$ were considered statistically significant. All experiments were performed at least three times.

Results

Generation of $Hzf^{-/-}$ Mutant Mice. The *Hzf* gene was disrupted in murine ES cells using a targeting vector in which the exons encoding three zinc finger motifs were deleted (Materials and Methods, and Fig. 1 A). The targeting vector was electroporated into R1 ES cells. After positive-negative selection and genotyping by Southern blot analysis as described in Materials and Methods, six independent clones were identified as heterozygous for the targeted mutation at the *Hzf* locus. Three out of the six heterozygous mutant ES clones were used to generate chimeric mice. Chimeras were backcrossed to CD1 mice to generate mice heterozygous for the *Hzf* mutation. Heterozygous $Hzf^{+/-}$ mice were fertile and were intercrossed to generate homozygous $Hzf^{-/-}$ mice (Fig. 1 B). The null mutation of *Hzf* was confirmed by the absence of *Hzf* expression, as determined by Northern blot analysis of RNA extracted from brains of *Hzf* mutant mice at 3 wk after birth (Fig. 1 C).

Hemorrhage and Neonatal Lethality of $Hzf^{-/-}$ Mice. Initial examination of the progeny from $Hzf^{+/-}$ parents revealed a reduced frequency of $Hzf^{-/-}$ mice at 3 wk of age. To determine the stage of neonatal development affected by the *Hzf* mutation, neonatal genotyping was performed. Of 300 offspring derived from heterozygous matings, 1-wk-old $Hzf^{-/-}$ pups were viable, usually of normal size, and were present in the expected Mendelian frequency. However, thereafter, especially between 2–3 wk after birth, the percentage of homozygotes decreased (Table I).

As shown in Fig. 2 A, the size of 4-wk-old $Hzf^{-/-}$ mice were clearly distinguishable from their wild-type littermates. Moreover, there was marked internal hemorrhaging evident primarily in the brains and gastrointestinal tracts (Fig. 2 B, and data not shown) in mutant neonates. This hemorrhaging was the likely cause of neonatal lethality. The surviving $Hzf^{-/-}$ mice of either sex were fertile (data not shown).

Unstable Hemostatic Plug Formation and Abnormal Platelet Morphology in $Hzf^{-/-}$ Mice. To determine whether the hemorrhaging phenotype was related to defective hemostasis in *Hzf*-deficient mice, we compared the bleeding times and rebleeding occurrences of $Hzf^{+/+}$, $Hzf^{+/-}$, and $Hzf^{-/-}$ mice. There were no significant differences in bleeding

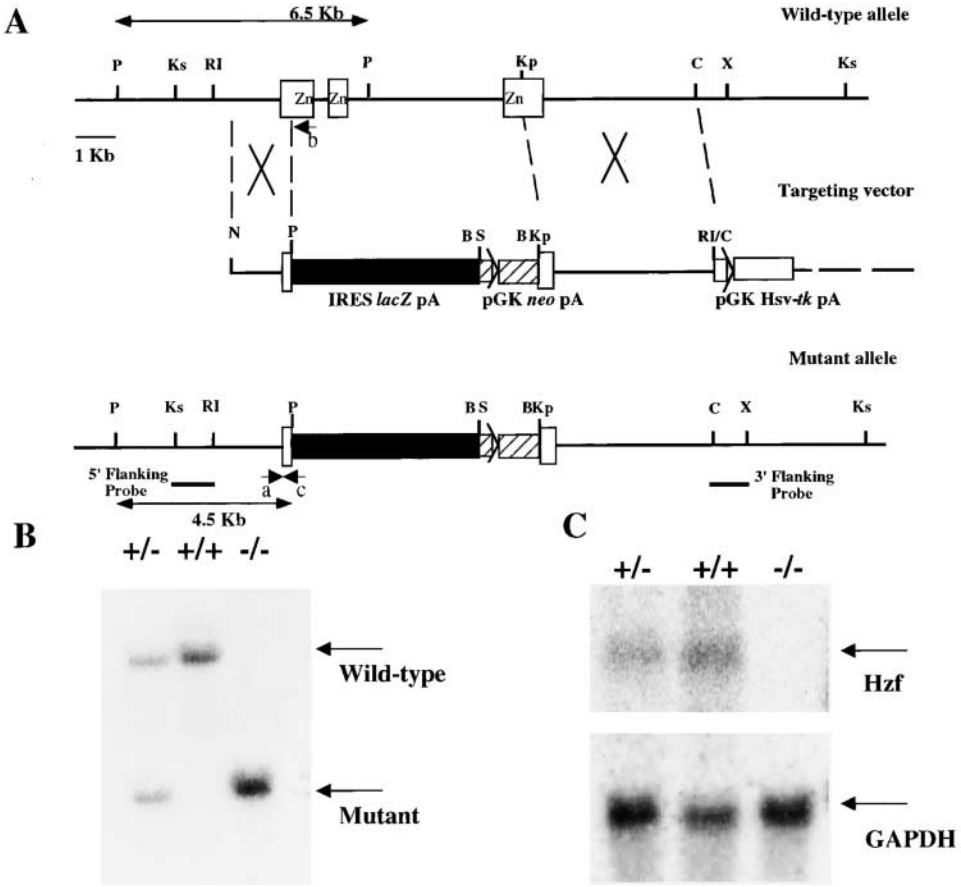

Figure 1. Targeted disruption of the *Hzf* locus. (A) A portion of the mouse 129/Sv *Hzf* wild-type locus (top) showing exons (open boxes) and a 6.5-kb PstI fragment in the wild-type allele. The targeting vector (middle) was designed to replace exons encoding three zinc finger domains with an IRES *Lac*Z (closed box) and a *neo* (hatched box). The mutated *Hzf* locus (bottom) contains a 4.5-kb PstI fragment. The positions of the 5′ flanking and 3′ flanking probes used for Southern blot analysis are shown. Positions of PCR primers for the wild-type allele (a and b) and the mutant allele (c) are also shown. P, Ks, RI, Kp, C, X, and B represent PstI, KspI, EcoRI, KpnI, ClaI, XhoI, and BamHI sites, respectively. (B) Genomic DNA was isolated from $Hzf^{+/+}$, $Hzf^{+/-}$, and $Hzf^{-/-}$ mice, digested with PstI and analyzed by Southern blot analysis. Wild-type (6.5-kb) and mutant (4.5-kb) bands are indicated. (C) Northern blot analysis of *Hzf* expression. Total RNA extracted from the brains (40 μg per lane) was analyzed for the expression of transcripts corresponding to the *Hzf* gene.

times when $Hzf^{-/-}$ mice were compared with wild-type and $Hzf^{+/-}$ heterozygous mice (Fig. 3 A). However, $Hzf^{-/-}$ mice rebled after transient hemostasis relative to the rebleeding frequency in wild-type and $Hzf^{+/-}$ mice (Fig. 3 B). These results indicate that *Hzf*-deficiency leads to unstable hemostatic plug formation in vivo.

Table I. *Genotype Analysis of the Progeny from Hzf Heterozygous Intercrosses*

	Number of mice of each genotype				Percentage
Stage	+/+	+/−	−/−	Total	−/−
					%
1 wk	10	22	12	44	27
2 wk	6	22	8	36	22
3 wk	32	90	24	146	16
4 wk	16	27	10	53	19
Total				295	

Breeding pairs were set up between $Hzf^{+/-}$ males and females (129 × CD1 mixed background). Tails of newborn and weaning pups were collected at the time of 1, 2, 3, and 4 wk after birth. The genotypes were determined by PCR analyses, as described in Materials and Methods. Each genotyping was confirmed by Southern blot analyses.

The defects in hemostasis in $Hzf^{-/-}$ mice led us to analyze hematologic parameters in $Hzf^{-/-}$ mice. Surprisingly, complete hematologic profiles revealed no significant differences in platelet counts and differential counts between $Hzf^{-/-}$ mice and their control littermates (data not shown).

To address the defect of hemostasis in detail, we next examined the morphology of blood cells in peripheral blood smears from $Hzf^{-/-}$ mice. Normal platelet sizes from control mice were observed by comparison with the diameter of erythrocytes (Fig. 3 C). Large faint-colored platelets were occasionally observed in blood smears from $Hzf^{-/-}$ mice (Fig. 3 D). Although the frequency of these pale ghostlike platelets was low, they were never observed in peripheral blood smears from $Hzf^{+/+}$ mice. To examine these morphological differences more closely, we performed ultrastructural analysis of peripheral platelets from $Hzf^{-/-}$ and control mice. As shown in Fig. 3 E, platelets from wild-type mice had easily identified dense α-granules. In contrast, $Hzf^{-/-}$ platelets had significantly reduced numbers of α-granules, with many vacuoles (Fig. 3 F; vacant frequency of α-granules, 9.4 ± 15.4 [controls] vs. 80.6 ± 12.3 [$Hzf^{-/-}$], $n = 11$, $P < 0.0001$).

Numerous procoagulant substances are packed in platelet α-granules, and the release of granule contents is important for platelet function (33). vWF, one of the procoagulant substances contained in platelet α-granules, is associated

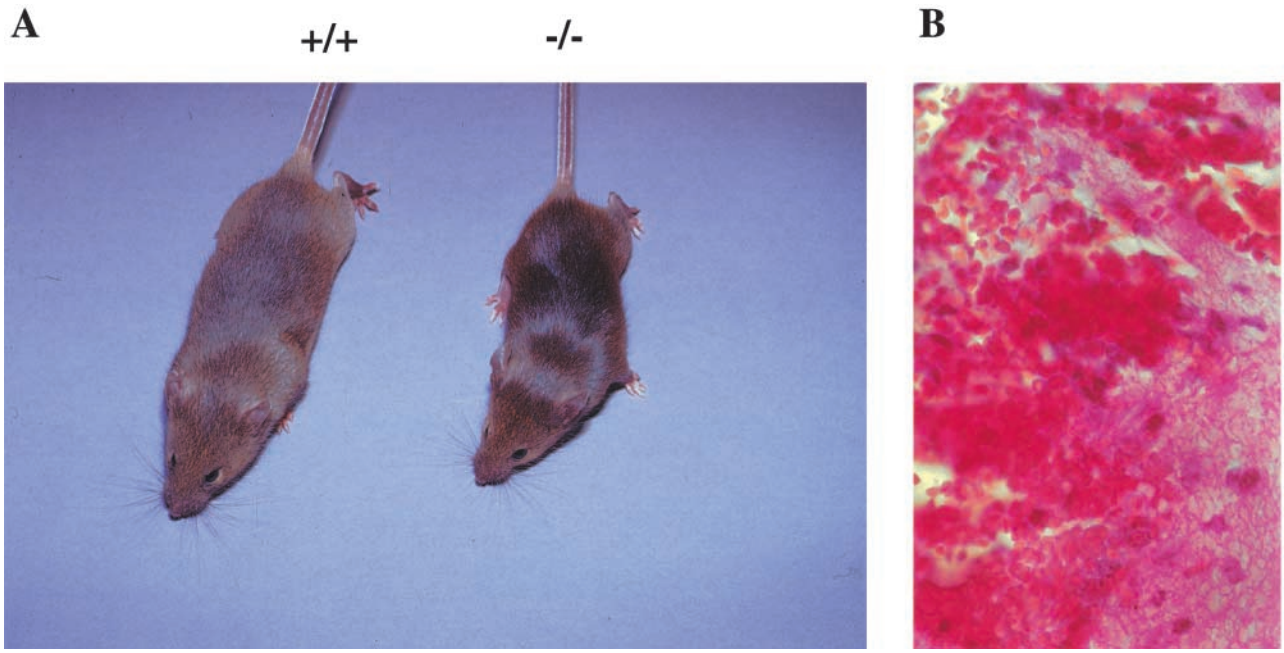

Figure 2. Growth retardation and hemorrhage in $Hzf^{-/-}$ mice. (A) A $Hzf^{-/-}$ mouse compared with a control littermate 4 wk after birth, demonstrating slightly smaller size. (B) Transverse section of the brain of a 3-wk-old $Hzf^{-/-}$ mouse, demonstrating extensive hemorrhage. Original magnification: ×100.

with attachment of platelets onto damaged blood vessels, thereby reinforcing the stability of the plug, and activating the coagulation pathway that leads to blood clot formation (33). To investigate whether α-granules in $Hzf^{-/-}$ platelets contain α-granule substances, we examined the protein levels of platelet-vWF, a key GP involved in coagulation. As shown in Fig. 3 G, the levels of vWF were dramatically reduced in $Hzf^{-/-}$ platelets compared with that observed in platelets from wild-type mice.

Number and DNA Ploidy Levels of Megakaryocytes and Megakaryocyte Progenitors from $Hzf^{-/-}$ Mice. To explore in greater detail the nature of the platelet defects described above, we characterized megakaryocytes from $Hzf^{-/-}$ mutant mice. No differences in the numbers of megakaryocytes were observed in the spleens and bone marrows of *Hzf* mutant mice, as determined morphologically and by flow cytometric analysis (Fig. 4 A–E).

Megakaryocyte development initiates with proliferation of precursor cells. These precursor cells then undergo endomitosis, followed by cytoplasmic maturation and organization, culminating in platelet release (1). To determine whether the process of endomitosis was affected by the absence of *Hzf*, we performed DNA ploidy analysis on bone marrow megakaryocytes. As shown in Fig. 4 F, no significant differences in DNA ploidy patterns were observed between wild-type, heterozygous, and homozygous mutant mice. We next examined the levels of megakaryocyte progenitor cells (CFU-Mk) in the bone marrow of *Hzf* wild-type and mutant mice by plating bone marrow cells in semi-solid media in the presence of TPO/MGDF. Normal numbers of megakaryocyte progenitors were observed in *Hzf*-deficient mice (data not shown).

Ultrastructural Analysis of Megakaryocytic Abnormality. To characterize further the maturation defect in $Hzf^{-/-}$ mice, we performed electron microscopic analysis of megakaryocytes derived from $Hzf^{-/-}$ mice. As expected, megakaryocytes from both $Hzf^{+/+}$ and $Hzf^{-/-}$ mice exhibited hyperlobulated nuclei (Fig. 5 A and B). Megakaryocytes from $Hzf^{+/+}$ mice exhibited well-formed platelet fields, demarcation membrane systems, and numerous α-granules (Fig. 5 C); in contrast, $Hzf^{-/-}$ megakaryocytes displayed a dramatic reduction in the number of α-granules, with many vacuoles in their cytoplasm (Fig. 5 D). Furthermore, detailed ultrastructural analysis revealed that α-granules in megakaryocytes from control mice were dense, readily identifiable, and exhibited distinct zones: dense nucleoid regions and diffuse granular matrixes (Fig. 5 E). In contrast, the α-granules in $Hzf^{-/-}$ megakaryocytes were pale and vacant, although membranes of α-granules could be identified (Fig. 5 F). In addition, the majority of $Hzf^{-/-}$ α-granules were devoid of diffuse granular matrixes, although dense nucleoid regions were observed only in some α-granules in $Hzf^{-/-}$ megakaryocytes (Fig. 5 F).

Taken together, these data suggest that the process of endomitosis is not affected by *Hzf*-deficiency. However, *Hzf*-deficiency appears to block the process of terminal maturation of megakaryocytes, affecting the assembly of α-granule substances in α-granules of megakaryocytes.

Reduced Concentrations of α-Granule Substances in $Hzf^{-/-}$ Megakaryocytes. Previous biochemical and immunoelectron microscopic analyses have shown that megakaryocytic α-granules contain numerous substances essential to the coagulation system (3). To examine the effect of *Hzf*-

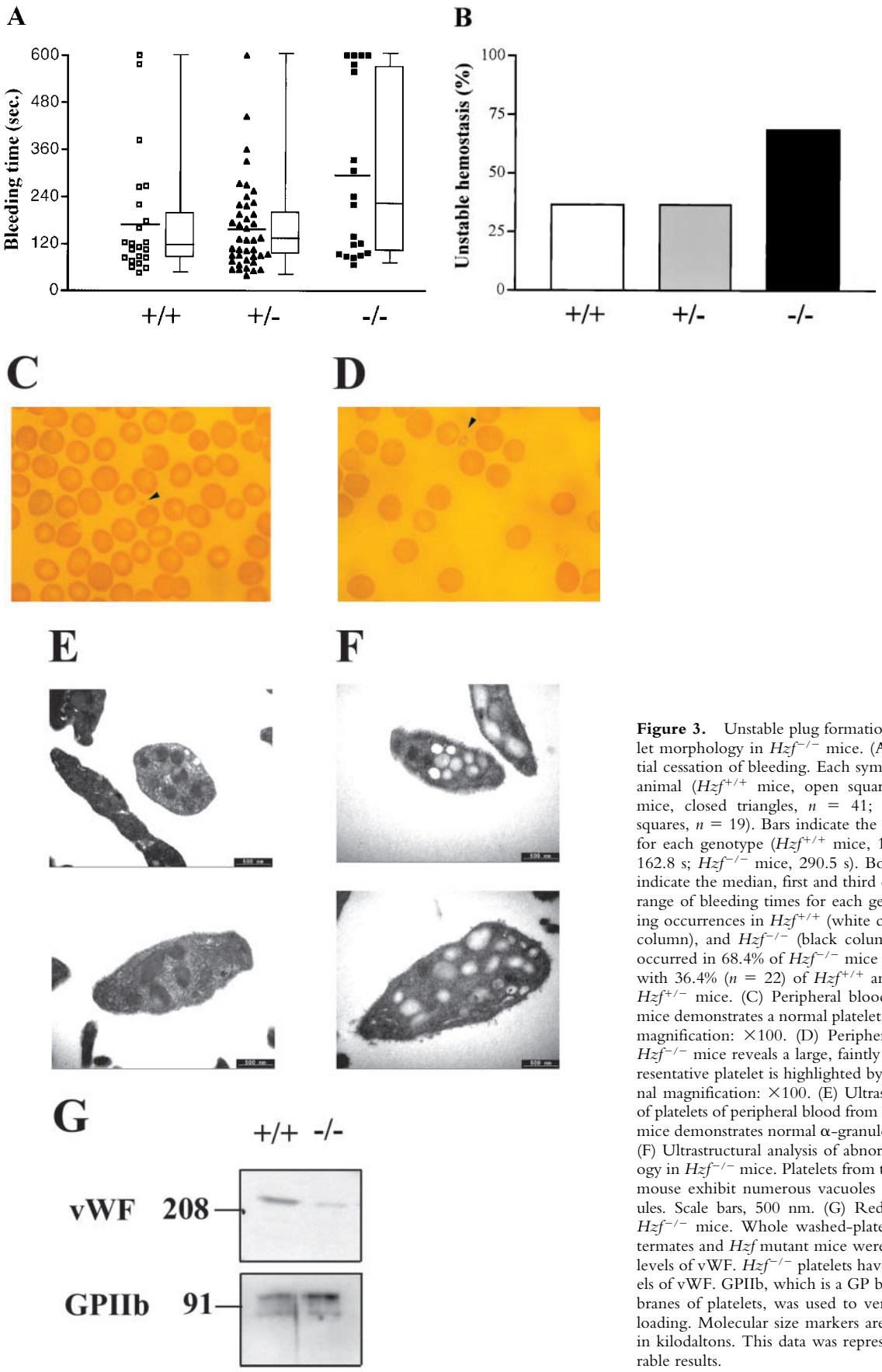

Figure 3. Unstable plug formation and abnormal platelet morphology in $Hzf^{-/-}$ mice. (A) Time taken for initial cessation of bleeding. Each symbol represents a single animal ($Hzf^{+/+}$ mice, open squares, $n = 22$; $Hzf^{+/-}$ mice, closed triangles, $n = 41$; $Hzf^{-/-}$ mice, closed squares, $n = 19$). Bars indicate the average bleeding time for each genotype ($Hzf^{+/+}$ mice, 177.0 s; $Hzf^{+/-}$ mice, 162.8 s; $Hzf^{-/-}$ mice, 290.5 s). Box and whisker graphs indicate the median, first and third quartiles, and the total range of bleeding times for each genotype. (B) Rebleeding occurrences in $Hzf^{+/+}$ (white column), $Hzf^{+/-}$ (gray column), and $Hzf^{-/-}$ (black column) mice. Rebleeding occurred in 68.4% of $Hzf^{-/-}$ mice ($n = 19$) as compared with 36.4% ($n = 22$) of $Hzf^{+/+}$ and 36.6% ($n = 41$) of $Hzf^{+/-}$ mice. (C) Peripheral blood smear from $Hzf^{+/+}$ mice demonstrates a normal platelet (arrowhead). Original magnification: ×100. (D) Peripheral blood smear from $Hzf^{-/-}$ mice reveals a large, faintly stained platelet. Representative platelet is highlighted by an arrowhead. Original magnification: ×100. (E) Ultrastructural morphology of platelets of peripheral blood from two individual $Hzf^{+/+}$ mice demonstrates normal α-granules. Scale bars, 500 nm. (F) Ultrastructural analysis of abnormal platelet morphology in $Hzf^{-/-}$ mice. Platelets from two individual $Hzf^{-/-}$ mouse exhibit numerous vacuoles with reduced α-granules. Scale bars, 500 nm. (G) Reduced platelet-vWF in $Hzf^{-/-}$ mice. Whole washed-platelets from control littermates and *Hzf* mutant mice were used to assay protein levels of vWF. $Hzf^{-/-}$ platelets have reduced protein levels of vWF. GPIIb, which is a GP bound to plasma membranes of platelets, was used to verify equivalent sample loading. Molecular size markers are indicated on the left in kilodaltons. This data was representative with comparable results.

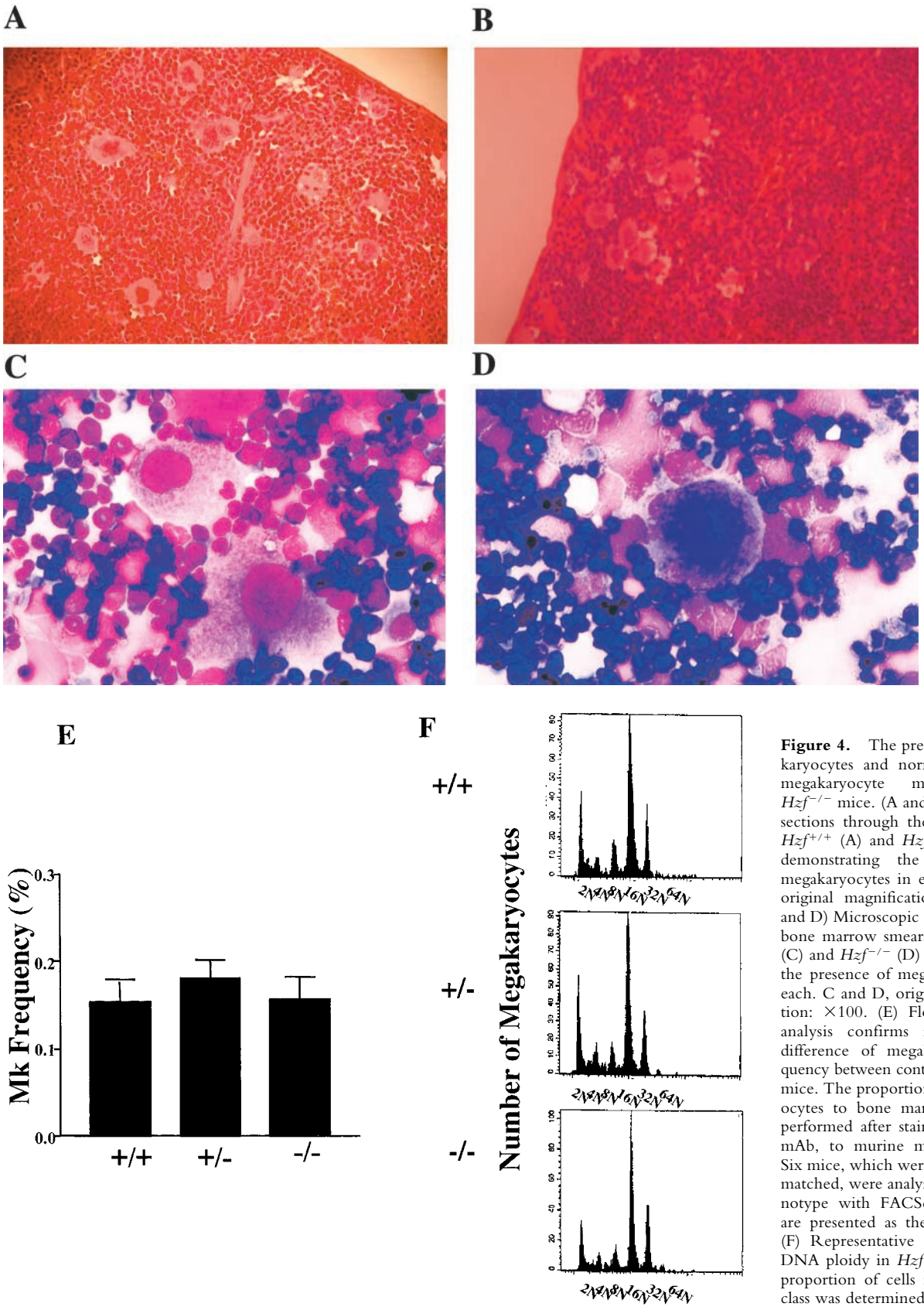

Figure 4. The presence of megakaryocytes and normal aspects of megakaryocyte maturation in $Hzf^{-/-}$ mice. (A and B) Transverse sections through the spleens from $Hzf^{+/+}$ (A) and $Hzf^{-/-}$ (B) mice, demonstrating the presence of megakaryocytes in each. A and B, original magnification: ×100. (C and D) Microscopic examination of bone marrow smears from $Hzf^{+/+}$ (C) and $Hzf^{-/-}$ (D) mice, showing the presence of megakaryocytes in each. C and D, original magnification: ×100. (E) Flow cytometric analysis confirms no significant difference of megakaryocyte frequency between control and $Hzf^{-/-}$ mice. The proportion of megakaryocytes to bone marrow cells was performed after staining with 4A5 mAb, to murine megakaryocytes. Six mice, which were age- and sex-matched, were analyzed in each genotype with FACScan™. Results are presented as the means ±SD. (F) Representative megakaryocyte DNA ploidy in $Hzf^{-/-}$ mice. The proportion of cells in each ploidy class was determined by PI-staining after gated on 4A5-positive cells with FACScan™, demonstrating no effect of *Hzf* deficiency on endomitosis. Six mice, which were age- and sex-matched, were analyzed in each genotype. This data was representative with comparable results.

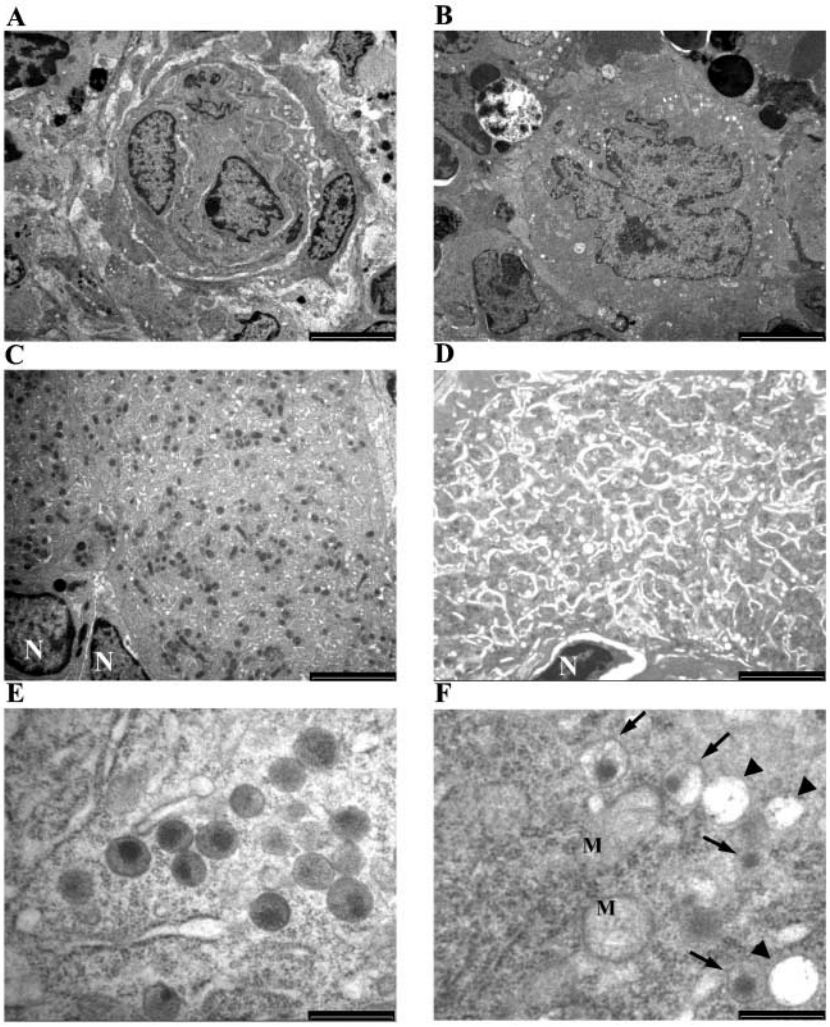

Figure 5. Ultrastructural analysis of megakaryocytic abnormality. (A and B) Mature megakaryocytes from the bone marrow of both $Hzf^{+/+}$ (A) and $Hzf^{-/-}$ (B) mice exhibit hyperlobulated nuclei. A and B, scale bars, 5,000 nm. (C) Detail of the cytoplasm of the megakaryocyte shown in A. Platelet fields or territories are clearly demarcated. Many α-granules are observed. N, nuclei. Scale bar, 2,500 nm. (D) Detail of the cytoplasm of the megakaryocyte shown in B. The $Hzf^{-/-}$ megakaryocyte reveals reduced numbers of α-granules, with many vacuoles. N, nucleus. Scale bar, 2,500 nm. (E) Ultrastructural analysis of α-granules of the megakaryocyte from $Hzf^{+/+}$ mice. Normal dense α-granules, which exhibits distinct zones: dense nucleoid regions and diffuse granular matrixes are observed. Scale bar, 500 nm. (F) Ultrastructural analysis of α-granules of the megakaryocytes from $Hzf^{-/-}$ mice. Some vacuoles (arrowheads) and low dense α-granules (arrows) are present in cytoplasm. M, mitochondria, in which cristae are observed. Scale bar, 500 nm.

deficiency on production of α-granule substances in megakaryocytes, we analyzed the levels of vWF, fibrinogen, PGDF-A, and PDGF-B by Western immunoblotting. As shown in Fig. 6 A, the levels of adhesive GP, vWF and fibrinogen, were both dramatically reduced in $Hzf^{-/-}$ bone marrow. In addition, *Hzf*-deficient bone marrow had significantly decreased protein levels of PDGF-A and PDGF-B.

To examine further the effect of *Hzf* deficiency on the levels of α-granule substances in megakaryocytes, we performed immunogold labeling followed by transmission electron microscopy. Using this strategy, we observed concentrated gold particles corresponding to PDGF-A in α-granules and on vesicles in the cytoplasm of $Hzf^{+/+}$ megakaryocytes (Fig. 6 B; numbers of PDGF-A gold particles in $Hzf^{+/+}$ α-granules: 19.8 ± 5.7%, $n = 5$). In contrast, PDGF-A was not detected in α-granules from $Hzf^{-/-}$ megakaryocytes although a few gold particles were present on vesicles (Fig. 6 C; PDGF-A gold particles in $Hzf^{-/-}$ α-granules: 0.8 ± 1.8%, $n = 5$, $P = 0.001$).

Transcript Levels of Megakaryocyte-specific Genes. To determine whether the structural defects observed in megakaryocytes from $Hzf^{-/-}$ mice were the consequence of an earlier block in megakaryocyte maturation, we examined the expression of two genes associated with megakaryopoiesis (29). In this experiment, bone marrow cells from mutant and wild-type male mice were used as the source of mRNAs for comparison of expression levels of the coadhesive GP, vWF, and the cell surface receptor, GPIIb. As shown in Fig. 7, $Hzf^{-/-}$ megakaryocytes expressed an equivalent level of RNA transcripts corresponding to GPIIb as $Hzf^{+/+}$ cells. In contrast, transcripts corresponding to vWF gene were significantly reduced in $Hzf^{-/-}$ cells relative to that observed in wild-type cells.

Discussion

We have previously identified a novel gene, *Hzf*, by a gene trapping strategy in ES cells (24). *Hzf* encodes a novel protein containing three C_2H_2-type zinc fingers and is predominantly expressed in megakaryocytes within the hematopoietic system. In this study, we have investigated the in vivo role of *Hzf* in mice using gene targeting. *Hzf* deficiency causes a block in the formation of

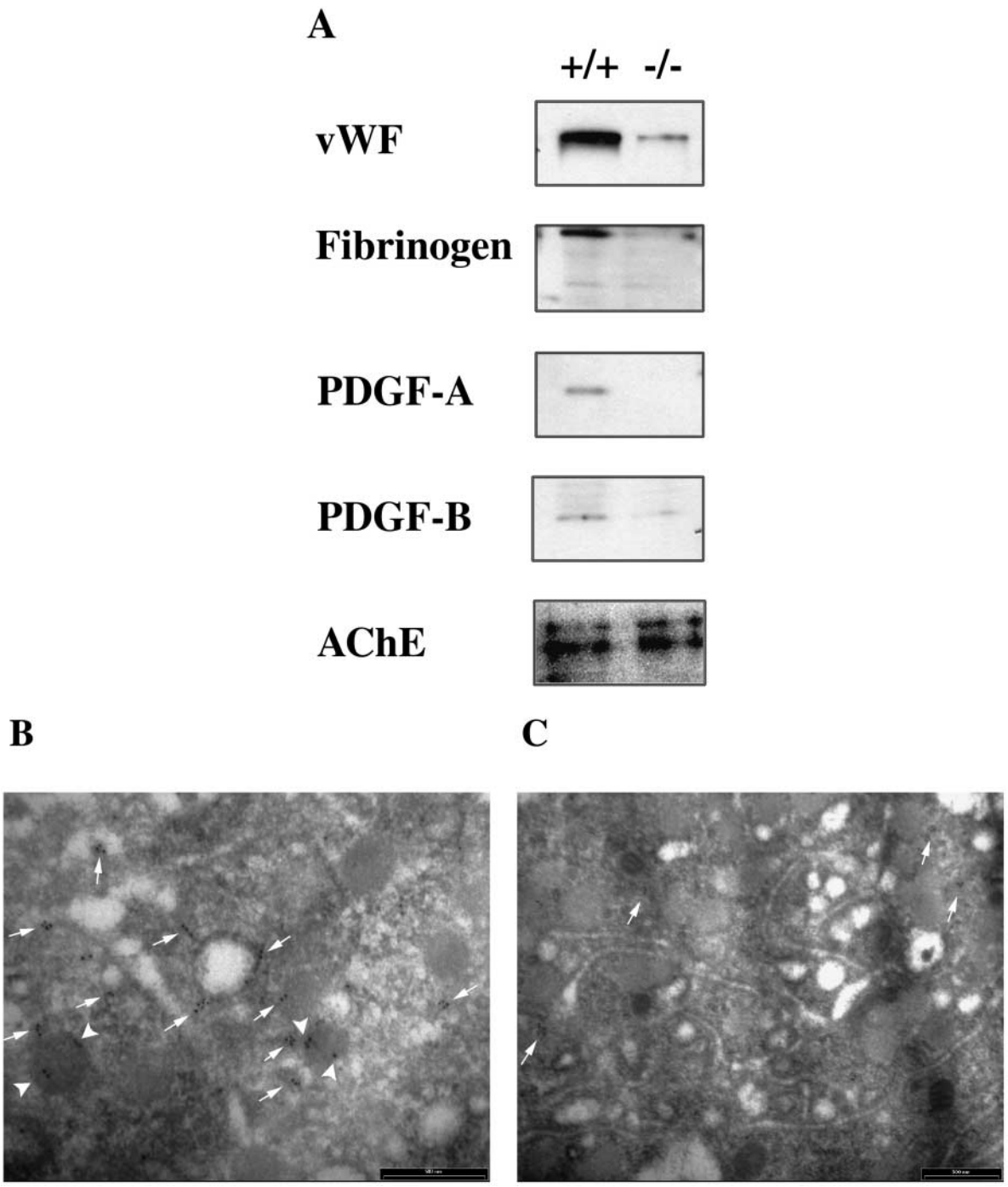

Figure 6. Reduced concentrations of α-granule substances in megakaryocytes from $Hzf^{-/-}$ mice. (A) Western immunoblotting analysis reveals reduced levels of vWF, fibrinogen, PDGF-A, and PDGF-B from bone marrow cells in $Hzf^{-/-}$ mice. The AChE, a house keeping protein expressed specifically in megakaryoctes, was used to verify equivalent sample loading. This data was representative with comparable results. (B and C) Immunogold localization of PDGF-A on thin sections of megakaryocytes in the spleens of $Hzf^{+/+}$(B) and $Hzf^{-/-}$ (C) mice. (B) Concentrated gold particles are located in the α-granules (arrowheads) and vesicles (arrows) of cytoplasm in megakaryocytes from $Hzf^{+/+}$ mice. Scale bar, 500 nm. (C) A few gold particles are present on the vesicles (arrows) of cytoplasm in megakaryocytes from $Hzf^{-/-}$ mice. Partially empty α-granules and vacant α-granules are also observed. Scale bar, 500 nm.

α-granules in megakaryocytes, abnormal platelet morphology, and disruption of hemostasis in vivo. These findings identify *Hzf* as a novel regulator of megakaryopoiesis and hemostasis.

Megakaryocyte Development and α-Granule Formation in Hzf-deficient Mice. Megakaryocytes in $Hzf^{-/-}$ mice were produced in normal number and appeared to undergo complete differentiation based on DNA ploidy analysis.

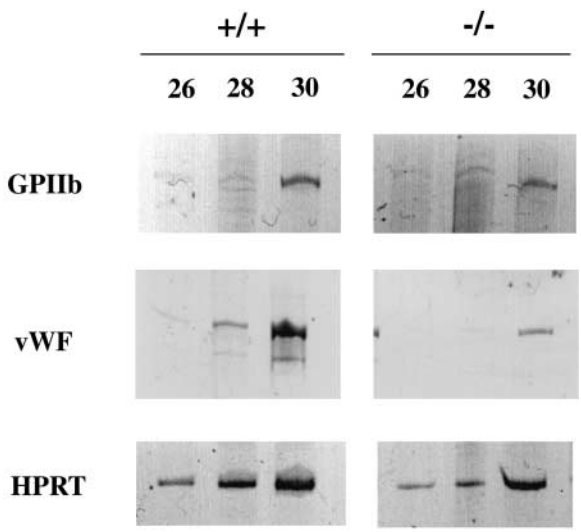

Figure 7. Down-regulation of megakaryocyte-specific gene expression in $Hzf^{-/-}$ mice. RT-PCR analysis of megakaryocyte-specific mRNAs from bone marrow cells of male $Hzf^{+/+}$ and $Hzf^{-/-}$ mice. Expression of indicated gene expression was determined by RT-PCR with indicated number of cycles and PAGE. Hypoxanthine phosphoribosyl transferase signal was used to equivalent cDNA amounts between male wild-type and male *Hzf* mutant.

Electronmicroscopic analysis revealed the presence of polyploid nuclei and the characteristic demarcation membrane system in megakaryocytes lacking HZF. Together, these findings suggest that *Hzf*-deficiency does not cause a block in the intermediate and late stages of megakaryocyte differentiation. The numbers of megakaryocyte progenitor cells were also not affected by the absence of *Hzf*, suggesting that *Hzf* is not essential for the early stages of megakaryocyte differentiation.

The electronmicroscopic and biochemical analyses revealed that platelets and megakaryocytes from $Hzf^{-/-}$ mice contain numerous vacuoles with reduced amount of α-granule substances. Interestingly, membranes of α-granules were observed in $Hzf^{-/-}$ megakaryocytes. In addition, PDGF-A was not detected in the α-granules of $Hzf^{-/-}$ megakaryocytes although a few gold particles were present on vesicles. Interestingly, immunoelectron microscopic analysis shows that vWF is detected on small vesicles of human cultured megakaryocytes (34). These findings suggest that *Hzf* is required for the synthesis of α-granule substances and/or the trafficking of these substances into α-granule bags during the process of megakaryocyte maturation.

Hzf in Platelet Morphogenesis and Hemostasis. Most $Hzf^{-/-}$ mice were smaller than their wild-type littermates, presumably as a result of sustained hemorrhage during a period of rapid growth. Because the numbers of platelets in *Hzf* mutant mice were within normal range, HZF does not appear to impair the release of platelets from megakaryocytes. Nevertheless, circulating large, faintly stained platelets containing numerous empty vacuoles were present in the peripheral blood of $Hzf^{-/-}$ mice.

Platelets from $Hzf^{-/-}$ mice have dramatically reduced levels of the coadhesive GPs, vWF and fibrinogen. vWF and fibrinogen contribute to hemostasis by producing a platelet plug and then reinforcing the plug by converting fibrinogen to fibrin strands, inducing activation of the coagulation pathway (33, 35). It is also known that GPIb, which is a heterodimer of GPIbα and GPIbβ, has an important role in the adherence of platelets to subendothelial surfaces with binding to vWF (35–37). Indeed, $vWF^{-/-}$ platelets exhibit delayed adhesion to vessel walls and they failed to form thromba in arterioles in vivo (38, 39). Thus, the instability of plug formation in *Hzf*-deficient mice may result from a failure of platelet adhesion onto damaged blood vessel walls, a process which is mediated by the binding of vWF to GPIb.

Gray Platelet Syndrome and Hzf Deficiency. It is of interest to note that the phenotype of the $Hzf^{-/-}$ mice described here resembles that observed in patients with gray platelet syndrome (GPS), a human congenital bleeding disorder (40, 41). Platelets from patients with GPS appear gray and are markedly deficient in morphologically dense α-granules and in the α-granule substances, β-thromboglobulin, fibrinogen, vWF, and PDGF (42–45). These similarities raise the intriguing possibility that GPS may be associated with defects in the biochemical pathway defined by HZF.

Gene Regulation by Hzf. The generation of mice with targeted mutations in specific genes has greatly enhanced our understanding of megakaryocyte differentiation. RNA transcripts for the vWF gene were significantly reduced in bone marrow cells derived from $Hzf^{-/-}$ mice. Thus, these results suggest either that *Hzf* directly regulates the expression of *vwf* and/or that delayed or incomplete maturation of megakaryocytes as a result of *Hzf* deficiency is reflected in decreased expression levels of *vwf* transcripts.

Taken together, this data suggests that *Hzf* plays an essential role in hemostasis in vivo through its direct or indirect regulation of the levels of at least one molecule, vWF known to be involved in plug formation through the adhesion of platelets to endothelial cells. We conclude that the defects in *Hzf*-deficient mice reflect, at least in part, a direct or indirect role for *Hzf* in vWF regulation.

We thank Sandra Tondat for ES cell aggregations, Lynda Doughty for DNA sequences, Ken Harpal for sectioning of tissues, Shirly Vesely, and George Cheong for preparation of reagents, Dr. Pascale Marchot for information on AChE, Drs. Denisa D. Wagner, Yoshiyasu Aoki, and anonymous reviewers for giving valuable comments, Lawrence Ng, Drs. Jerry Ware, Akira Suzuki, Ryuichi Sakai, Takehiro Kawano, Seiji Tadokoro, Sanford J. Shattil, and Ramesh A. Shivdasani for technical advice, Bev Bessey for administrative support, and Drs. Mira Puri, Cindy Todoroff, and Kazunobu Tachibana for reviewing the manuscript.

This work was supported by grants from the National Cancer Institute of Canada and the Terry Fox Cancer Foundation (to A. Bernstein) and in part by grants p30CA21765 and p01CA20180 from the National Cancer Institute, U.S. Public Health Service, Department of Health and Human Services, and by the American Lebanese Syrian Associated Charities (to C.W. Jackson). Y. Kimura

was supported by the Mochida Memorial Foundation for Medical and Pharmaceutical Research.

Submitted: 4 September 2001
Revised: 19 February 2002
Accepted: 1 March 2002

References

1. Zuker-Franklin, D. 1989. Megakaryocytes and platelets. *In* Atlas of Blood Cells: Function and Pathology. D. Zuker-Franklin, M.F. Greaves, C.E. Grossi, and A.M. Marmont, editors. Lea and Feiger, Philadelphia. pp. 621–693.
2. Jackson, C.W., L.K. Brown, B.C. Somerville, S.A. Lyles, and A.T. Look. 1984. Two-color flow cytometric measurement of DNA distributions of rat megakaryocytes in unfixed, unfractionated marrow cell suspensions. *Blood.* 63:768–778.
3. Burstein, S.A., and J. Breton-Gorius. 1995. Megakaryopoiesis and platelet formation. 5th ed. *In* Williams Hematology. E. Beutler, M.A. Litchtman, B.S. Coller, and T.J. Kipps, editors. McGraw-Hill, Inc., New York, NY. 1149–1160.
4. Greenberg, S.M., D.J. Kuter, and R.D. Rosenberg. 1987. *In vitro* stimulation of megakaryocyte maturation by megakaryocyte stimulatory factor. *J. Biol. Chem.* 262:3269–3277.
5. Shivdasani, R.A., M.F. Rosenblatt, D. Zucker-Franklin, C.W. Jackson, P. Hunt, C.J.M. Saris, and S.H. Orkin. 1995. Transcription factor NF-E2 is required for platelet formation independent of the actions of thrombopoietin/MGDF in megakaryocyte development. *Cell.* 81:695–704.
6. Shavit, J.A., H. Motohashi, K. Onodera, J. Akasaka, M. Yamamoto, and J.D. Engel. 1998. Impaired megakaryopoiesis and behavioral defects in *maf*G-null mutant mice. *Genes Dev.* 12:2164–2174.
7. Shivdasani, R.A., Y. Fujiwara, M.A. McDevitt, and S.H. Orkin. 1997. A lineage-selective knockout establishes the critical role of transcription factor GATA-1 in megakaryocyte growth and platelet development. *EMBO J.* 16:3965–3973.
8. Hart, A., F. Melet, P. Grossfeld, K. Chien, C. Jones, A. Tunnacliffe, R. Favier, and A. Bernstein. 2000. *Fli*-1 is required for murine vascular and megakaryocytic development and is hemizygously deleted in patients with thrombocytopenia. *Immunity.* 13:167–177.
9. Blank, V., and N.C. Andrews. 1997. The Maf transcription factors: Regulators of differentiation. *Trends Biochem. Sci.* 22: 437–441.
10. Motohashi, H., J.A. Shavit, K. Igarashi, M. Yamamoto, and J.D. Engel. 1997. The world according to Maf. *Nucleic Acids Res.* 25:2953–2959.
11. Souyri, M., I. Vigon, J.-F. Penciolelli, J.-M. Heard, P. Tambourin, and F. Wendling. 1990. A putative truncated cytokine receptor gene transduced by the myeloproliferative leukemia virus immortalizes hematopoietic progenitors. *Cell.* 63: 1137–1147.
12. Bartley, T.D., J. Bogenberger, P. Hunt, Y.S. Li, H.S. Lu, F. Martin, M.S. Chang, B. Samal, J.L. Nichol, S. Swift, et al. 1994. Identification and cloning of a megakaryocyte growth and development factor that is a ligand for the cytokine receptor Mpl. *Cell.* 77:1117–1124.
13. de Sauvage, F.J., P.E. Hass, S.D. Spencer, B.E. Malloy, A.L. Gurney, S.A. Spencer, W.C. Darbonne, W.J. Henzel, S.C. Wong, W.-J. Kuang, et al. 1994. Stimulation of megakaryocytopoiesis and thrombopoiesis by the c-Mpl ligand. *Nature.* 369:533–538.
14. Kaushansky, K., S. Lok, R.D. Holly, V.C. Broudy, N. Lin, M.C. Bailey, J.W. Forstrom, M.M. Buddle, P.J. Oort, F.S. Hagen, G.J. Roth, T. Papayannopoulou, and D.C. Foster. 1994. Promotion of megakaryocyte progenitor expansion and differentiation by the c-Mpl ligand thrombopoietin. *Nature.* 369:568–571.
15. Kuter, D.J., D.L. Beeler, and R.D. Rosenberg. 1994. The purification of megapoietin: a physiological regulator of megakaryocyte growth and platelet production. *Proc. Natl. Acad. Sci. USA.* 91:11104–11108.
16. Lok, S., K. Kaushansky, R.D. Holly, J.L. Kuijper, C.E. Lofton-Day, P.J. Oort, F.J. Grant, M.D. Heipel, S.K. Burkhead, J.M. Kramer, et al. 1994. Cloning and expression of murine thrombopoietin cDNA and stimulation of platelet production *in vivo*. *Nature.* 369:565–568.
17. Wendling, F., E. Maraskovsky, N. Debili, C. Florindo, M. Teepe, M. Titeux, N. Methia, J. Breton-Gorius, D. Cosman, and W. Vainchenker. 1994. c-Mpl ligand is a humoral regulator of megakaryocytopoiesis. *Nature.* 369:571–574.
18. Kato, T., K. Ogami, Y. Shimada, A. Iwamatsu, Y. Sohma, H. Akahori, K. Horie, A. Kokubo, Y. Kudo, and E. Maeda. 1995. Purification and characterization of thrombopoietin. *J. Biochem.* 118:229–236.
19. Choi, E.S., M.M. Hokom, J.L. Chen, J. Skrine, J. Faust, J. Nichol, and P. Hunt. 1996. The role of megakaryocyte growth and development factor in terminal stages of thrombopoiesis. *Br. J. Haematol.* 95:227–233.
20. Gurney, A.L., K. Carver-Moore, F.J. de Sauvage, and M.W. Moore. 1994. Thrombocytopenia in c-*mpl*-deficient mice. *Science.* 265:1445–1447.
21. Alexander, W.S., A.W. Roberts, N.A. Nicola, R. Li, and D. Metcalf. 1996. Deficiencies in progenitor cells of multiple hematopoietic lineages and defective megakaryocytopoiesis in mice lacking the thrombopoietic receptor c-Mpl. *Blood.* 87:2162–2170.
22. de Sauvage, F.J., K. Carver-Moore, S.-M. Luoh, A. Ryan, M. Dowd, D.L. Eaton, and M.W. Moore. 1996. Physiological regulation of early and late stages of megakaryocytopoiesis by thrombopoietin. *J. Exp. Med.* 183:651–656.
23. Stanford, W.L., G. Caruana, K.A. Vallis, M. Inamdar, M. Hidaka, V.L. Bautch, and A. Bernstein. 1998. Expression trapping: identification of novel genes expressed in hematopoietic and endothelial lineages by gene trapping in ES cells. *Blood.* 92:4622–4631.
24. Hidaka, M., G. Caruana, W.L. Stanford, M. Sam, P.H. Correll, and A. Bernstein. 2000. Gene trapping of two novel genes, *Hzf* and *Hhl*, expressed in hematopoietic cells. *Mech. Dev.* 90:3–15.
25. Nieswandt, B., B. Echtenacher, F.-P. Wachs, J. Schroder, J.E. Gessner, R.E. Schmidt, G.E. Grau, and D.N. Mannel. 1999. Acute systemic reaction and lung alterations induced by an antiplatelet integrin gpIIb/IIIa antibody in mice. *Blood.* 94:684–693.
26. Dejana, E., A. Quintana, A. Callioni, and G. de Gaetano. 1979. Bleeding time in laboratory animals. III - Do tail bleeding times in rats only measure a platelet defect? (the aspirin puzzle). *Thromb. Res.* 15:199–207.
27. Law, D.A., F.R. DeGuzman, P. Heiser, K. Ministri-Madrid, N. Killeen, and D.R. Phillips. 1999. Integrin cytoplasmic tyrosine motif is required for outside-in αIIbβ3 signalling and platelet function. *Nature.* 401:808–811.
28. Arnold, J.T., N.C. Daw, P.E. Stenberg, D. Jayawardene,

D.K. Srivastava, and C.W. Jackson. 1997. A single injection of pegylated murine megakaryocyte growth and development factor (MGDF) into mice is sufficient to produce a profound stimulation of megakaryocyte frequency, size, and ploidization. *Blood.* 89:823–833.
29. Vyas, P., K. Ault, C.W. Jackson, S.H. Orkin, and R.A. Shivdasani. 1999. Consequences of GATA-1 deficiency in megakaryocytes and platelets. *Blood.* 93:2867–2875.
30. Berger, G., J.M. Masse, and E.M. Cramer. 1996. α-granule membrane mirrors the platelet plasma membrane and contains the glycoproteins Ib, IX, and V. *Blood.* 87:1385–1395.
31. Kimura, Y., K. Yamada, T. Sakai, K. Mishima, H. Nishimura, Y. Matsumoto, M. Singh, and Y. Yoshikai. 1998. The regulatory role of heat shock protein 70-reactive $CD4^+$ T cells during rat listeriosis. *Int. Immunol.* 10:117–130.
32. Fennie, C., J. Cheng, D. Dowbenko, P. Young, and L.A. Lasky. 1995. $CD34^+$ endothelial cell lines derived from murine yolk sac induce the proliferation and differentiation of yolk sac $CD34^+$ hematopoietic progenitors. *Blood.* 86:4454–4467.
33. Ware, J.A., and B.S. Coller. 1995. Platelet morphology, biochemistry, and function. *In* Williams Hematology. E. Beutler, M.A. Litchtman, B.S. Coller, and T.J. Kipps, editors. McGraw-Hill, Inc., New York, NY. 1161–1201.
34. Cramer, E.M., W. Vainchenker, G. Vinci, J. Guichard, and J. Breton-Gorius. 1985. Gray platelet syndrome: immunoelectron microscopic localization of fibrinogen and von Willebrand factor in platelets and megakaryocytes. *Blood.* 66:1309–1316.
35. Savage, B., E. Saldivar, and Z.M. Ruggeri. 1996. Initiation of platelet adhesion by arrest onto fibrinogen or translocation on von Willebrand factor. *Cell.* 84:289–297.
36. Sakariassen, K.S., P.M. Nievelstein, B.S. Coller, and J.J. Sixma. 1986. The role of platelet membrane glycoproteins Ib and IIb-IIIa in platelet adherence to human artery subendothelium. *Br. J. Haematol.* 63:681–691.
37. Parker, R.I., and H.R. Gralnick. 1987. Fibrin monomer induces binding of endogenous platelet von Willebrand factor to the glycocalicin portion of platelet glycoprotein Ib. *Blood.* 70:1589–1594.
38. Denis, C., N. Methia, P.S. Frenette, H. Rayburn, M. Ullman-Cullere, R.O. Hynes, and D.D. Wagner. 1998. A mouse model of severe von Willebrand disease: defects in hemostasis and thrombosis. *Proc. Natl. Acad. Sci. USA.* 95: 9524–9529.
39. Ni, H., C.V. Denis, S. Subbarao, J.L. Degen, T.N. Sato, R.O. Hynes, and D.D. Wagner. 2000. Persistence of platelet thrombus formation in arterioles of mice lacking both von Willebrand factor and fibrinogen. *J. Clin. Invest.* 106:385–392.
40. Raccuglia, G. 1971. Gray platelet syndrome: a variety of qualitative platelet disorder. *Am. J. Med.* 51:818–828.
41. White, J.G. 1979. Ultrastructural studies of the gray platelet syndrome. *Am. J. Pathol.* 95:445–462.
42. Gerrard, J.M., D.R. Phillips, G.H. Rao, E.F. Plow, D.A. Walz, R. Ross, L.A. Harker, and J.G. White. 1980. Biochemical studies of two patients with the gray platelet syndrome. Selective deficiency of platelet α granules. *J. Clin. Invest.* 66:102–109.
43. Levy-Toledano, S., J.P. Caen, J. Breton-Gorius, F. Rendu, C. Cywiner-Golenzer, E. Dupuy, Y. Legrand, and J. Maclouf. 1981. Gray platelet syndrome: α-granule deficiency: its influence on platelet function. *J. Lab. Clin. Med.* 98:831–848.
44. Nurden, A.T., T.J. Kunicki, D. Dupuis, C. Soria, and J.P. Caen. 1982. Specific protein and glycoprotein deficiencies in platelets isolated from two patients with the gray platelet syndrome. *Blood.* 59:709–718.
45. Berndt, M.C., P.A. Castaldi, S. Gordon, H. Halley, and V.J. McPherson. 1983. Morphological and biochemical confirmation of gray platelet syndrome in two siblings. *Aust. N.Z.J. Med.* 13:387–390.